Spin–orbit distortion of the hyperfine structure in heavier molecules: Breakdown of the case (aβ) formalism in the B 3Φ–X 3Δ system of gaseous NbN

Y. Azuma, J. A. Barry, M. P. J. Lyne, A. J. Merer, J. O. Schröder, and J.L. Féménias

Citation: The Journal of Chemical Physics **91**, 1 (1989); doi: 10.1063/1.457505
View online: http://dx.doi.org/10.1063/1.457505
View Table of Contents: http://scitation.aip.org/content/aip/journal/jcp/91/1?ver=pdfcov
Published by the AIP Publishing

Articles you may be interested in

SpinOrbital Function Formalism and ASPIRRIN Code
AIP Conf. Proc. **675**, 761 (2003); 10.1063/1.1607237

Hyperfine and spin–orbit structure of the 4Δ i ground state of CoO
J. Chem. Phys. **99**, 6336 (1993); 10.1063/1.465872

Hyperfine structure in the red emission system of NbN
J. Chem. Phys. **63**, 2861 (1975); 10.1063/1.431691

Theory of the Hyperfine Structure of Molecules: Application to 3Π States of Diatomic Molecules Intermediate between Hund's Cases (a) and (b)
J. Chem. Phys. **45**, 4214 (1966); 10.1063/1.1727481

On the Theory of SpinOrbit and Hyperfine Interactions in Molecules. Application to the Hydrogen Molecule—Ion
J. Chem. Phys. **37**, 485 (1962); 10.1063/1.1701362

This article is copyrighted as indicated in the article. Reuse of AIP content is subject to the terms at: http://scitation.aip.org/termsconditions. Downloaded to IP: 128.114.34.22 On: Wed, 26 Nov 2014 12:31:44

Spin–orbit distortion of the hyperfine structure in heavier molecules: Breakdown of the case (a_β) formalism in the $B\,^3\Phi$–$X\,^3\Delta$ system of gaseous NbN

Y. Azuma,[a] J. A. Barry,[b] M. P. J. Lyne, A. J. Merer, and J. O. Schröder[c]
Department of Chemistry, University of British Columbia, 2036 Main Mall, Vancouver, B.C. V6T 1Y6, Canada

J.-L. Féménias
Laboratoire d'Optique Atomique et Moléculaire, Université de Nice, Parc Valrose, 06034 Nice Cedex, France

(Received 1 February 1989; accepted 1 March 1989)

A detailed analysis of the rotational and hyperfine structure of the (0,0) band of the $B\,^3\Phi$–$X\,^3\Delta$ electronic transition of NbN has been performed from sub-Doppler spectra taken with linewidths of about 50 MHz. The Nb hyperfine structure is impressively wide in both states, but particularly so in $X\,^3\Delta$ where one of the unpaired electrons occupies a σ orbital derived from the metal 5*s* orbital. The electron spin and hyperfine structures do not follow the expected case (a_β) coupling because of extensive second order spin-orbit effects. It is shown that the asymmetry in the spin–orbit structure of $X\,^3\Delta$ is explained almost quantitatively by interaction with a $^1\Delta$ state from the same electron configuration (which lies at 5197 cm^{-1}); also cross terms between the spin–orbit and Fermi contact interactions in the matrix element $\langle {}^3\Delta_2|H|{}^1\Delta\rangle$ produce a large correction to the apparent coefficient of the **I**·**L** magnetic hyperfine interaction in $X\,^3\Delta_2$. The hyperfine structure in a triplet state turns out to be extremely sensitive to the details of the electron spin coupling, and reversals in the sense of the hyperfine structure in the $^3\Phi_4$–$^3\Delta_3$ and $^3\Phi_2$–$^3\Delta_1$ subbands are shown to be consistent with the $^3\Delta$ state being a regular spin–orbit multiplet ($A > 0$). Particular care has been taken with the calibration, which has meant that extra terms have needed to be added to the magnetic hyperfine Hamiltonian to account for the spin–orbit distortions: instead of the usual three parameters needed in case (a_β) coupling, the $B\,^3\Phi$ state has required four parameters and the $X\,^3\Delta$ state has required five. The model explains the data very well, and the standard deviation in the least-squares fit to more than 1000 hyperfine line frequencies was 0.000 58 cm^{-1} (17 MHz).

I. INTRODUCTION

The $^{93}_{41}$Nb nucleus has the largest magnetic moment of any nonradioactive atom and, with its spin $I = 9/2$, it produces some extraordinarily impressive hyperfine effects in the gas-phase optical spectra of its open shell compounds. The large size of the hyperfine splittings means that the uncertainties in the experimentally determined parameters are very much smaller than the parameters themselves; as a result, the hyperfine parameters, which are expectation values of functions of the electron coordinates near a spinning nucleus, give particularly accurate measures of the electronic properties for these molecules. Data of this type are valuable in testing the quality of *ab initio* wave functions and in modeling the chemical bonding.

With a nuclear spin I of 9/2 the complexity of the spectra is usually so great that analysis is not possible without detailed laser studies at very high resolution, though a few band systems are known where the structure is partially resolved with a grating spectrograph. Among these are the $C\,^4\Sigma^-$–$X\,^4\Sigma^-$ system of NbO[1–3] and the $B\,^3\Phi$–$X\,^3\Delta$ system of NbN.[4] Even so, the full extent of the hyperfine structure is best appreciated from sub-Doppler spectra where all the details can be seen.

This paper reports a high resolution study of the $B\,^3\Phi$–$X\,^3\Delta$ electronic transition of NbN near 6000 Å. The hyperfine structure has been analyzed in detail and, because the transition is unperturbed rotationally, it provides what will surely be one of the finest "textbook" examples of nuclear spin effects in a high multiplicity situation. The interpretation of the hyperfine structure is complicated by strong spin-orbit mixing between the $X\,^3\Delta$ state and the low-lying $a\,^1\Delta$ state from the same electron configuration; it is found that the standard case (a_β) form for the hyperfine Hamiltonian[5] breaks down severely, and a total of five hyperfine parameters is required for the $X\,^3\Delta$ state instead of the usual three. It is also found that the hyperfine structure is surprisingly sensitive to the details of the electron spin coupling. For in-

[a] Present address: Physics Division, Argonne National Laboratory, 9700 South Cass Avenue, Argonne, Illinois 60439.
[b] Present address: Dept. of Chemistry, University of Arizona, Tucson, Arizona 85721.
[c] Visiting from: Institut für Molekülphysik, Fachbereich Physik, Freie Universität Berlin, Arnimallee 14, D-1000 Berlin 33, Germany. Permanent address: Drägerwerk Aktiengesellschaft, Moislinger Allee 53/55 D-2400 Lübeck 1, Germany.

 0021-9606/89/130001-12$02.10 © 1989 American Institute of Physics

This article is copyrighted as indicated in the article. Reuse of AIP content is subject to the terms at: http://scitation.aip.org/termsconditions. Downloaded to IP: 128.114.34.22 On: Wed, 26 Nov 2014 12:31:44

stance, the ground state is an example of what is normally described as "good case (a) coupling", with a very large value of $Y = A/B$; no spin satellite branches, representing spin uncoupling towards case (b), are seen in the $B\,^3\Phi$–$X\,^3\Delta$ transition, and yet the hyperfine structure of the $X\,^3\Delta_1$ component shows a reversal in its energy order, characteristic of spin uncoupling, at a J value as low as 15.

II. EXPERIMENTAL

Gaseous niobium nitride was produced in a flow system by the action of a 2450 MHz electrodeless discharge on a mixture of $NbCl_5$ vapor, nitrogen, and argon. The $NbCl_5$ vapor was produced by warming a small quantity of solid $NbCl_5$, contained in a sidearm of the quartz discharge tube, to about 80 °C; it was then entrained in the flow of N_2 and Ar. The total pressure was slightly over 1 Torr. The discharge produced a bright lavender-colored flame, whose color corresponded to the electronic emission spectrum of NbN. This flame was pumped across a stainless steel fluorescence cell, fitted with Brewster angle windows and light baffles, through which a laser beam was passed. The arrangement was such that the laser beam crossed the tail of the flame, where most of the NbN molecules were in their ground electronic state, and the resulting fluorescence could be observed with a photomultiplier tube against a relatively dark background.

The laser used was a Coherent Inc. model 599-21 standing wave dye laser, operating with the dyes kiton red, rhodamine 6G, and rhodamine 110, which gives wavelength coverage from 6200 to 5300 Å. There was no need for laser powers higher than ~100 mW in the present experiments since the $B\,^3\Phi$–$X\,^3\Delta$ system of NbN is very strong. Broad-band spectra were taken (with the intracavity assembly of the laser removed) for the whole region, and selected regions were recorded at Doppler-limited resolution or at sub-Doppler resolution using the method of intermodulated fluorescence.[6] In these latter experiments the two chopper frequencies were in the ratio 7:9 and the sum frequency (near 1300 Hz) was used for demodulation.

Particular attention has been paid to the calibration. The spectra were recorded by scanning the dye laser frequency under the control of a PDP 11/23 minicomputer, which also acquired the absorption spectrum of iodine (for frequency standards[7]) and interpolation markers from a 299 MHz free spectral range Fabry–Perot interferometer. Our calibration method[8] concatenates a number of overlapping 35 GHz scans of the dye laser using the narrow lines of the intermodulated fluorescence spectrum to establish the relative order numbering of the interferometer markers in successive scans. Allowance is made for possible shifts in the frequencies of the markers caused by changes in the room temperature and pressure, or the angle of the laser beam entering the interferometer if the laser has to be realigned. It is then possible to carry out a least squares fit to the frequencies of all 30 or so iodine lines in a scan of some 10 cm^{-1} to establish the frequency of the first marker and the marker separation. Individual iodine lines (whose frequencies are taken from Gerstenkorn and Luc's atlas[7]) show residuals of up to ± 0.0025 cm^{-1}, but a graph of the residuals against frequency is a band of points whose center line can be accurately determined. Even though the iodine lines are about 0.03 cm^{-1} wide, the method gives a precision of about ± 0.0005 cm^{-1} (15 MHz) for the intermodulated fluorescence lines, as judged by the standard deviation of the least-squares fit.

The linewidths in our intermodulated fluorescence spectra are limited by the pressure in the fluorescence cell to about 50 MHz, but this is more than adequate to resolve most of the structure.

III. THE $B\,^3\Phi$–$X\,^3\Delta$ SYSTEM OF NbN

The $B\,^3\Phi$–$X\,^3\Delta$ system of NbN was first recorded photographically by Dunn and Rao in 1969.[9] The strongest bands form three $\Delta v = 0$ vibrational sequences, corresponding to the three triplet spin components; the rotational structure is almost undegraded. Considerable hyperfine splittings occur in the low J lines of the outer two spin components, which is consistent with both states belonging to case (a_β) spin coupling,[2] that is where

$$\mathbf{R} + \mathbf{L} + \mathbf{S} = \mathbf{J}; \quad \mathbf{J} + \mathbf{I} = \mathbf{F}. \tag{1}$$

The presence of the large hyperfine splittings had prevented analysis of all except the central component of the (0,0) band, $^3\Phi_3$–$^3\Delta_2$, where the hyperfine structure is much narrower. The details of the hyperfine splittings, as seen at grating resolution, were later studied by Féménias *et al.*[10] Their main conclusions were that there is significant hyperfine splitting in the low J levels of both the $^3\Phi$ and $^3\Delta$ electronic states, and that some of the high J lines are wider than expected from extrapolation of the low J structure, possibly indicating that spin uncoupling in one of the states causes further hyperfine effects.

Rotational analyses of the (0,0) band have recently been published by Pazyuk *et al.*[11] and Féménias *et al.*[4] A problem faced by both groups was that the magnitudes of the spin–orbit intervals were not known accurately. Féménias *et al.*[4] were able to estimate the spin–orbit intervals from the differences between the effective B values of the substates, but since these differences are quite small their estimates are good only to about 20%. Pazyuk *et al.*,[11] on the other hand, were misled by the presence in their spectra of two subbands of the weak $C\,^3\Pi$–$X\,^3\Delta$ system, which lie just to the blue of the $B\,^3\Phi$–$X\,^3\Delta$ bands, and which they assigned as $\Delta\Sigma \neq 0$ spin satellite subbands of the $B\,^3\Phi$–$X\,^3\Delta$ system; as a result their published values for the spin–orbit parameters are incorrect.

The exact sizes of the spin–orbit intervals have turned out to be very important in the detailed interpretation of the hyperfine structure described in this paper. Fortunately, they could be obtained from some extremely weak spin satellite branches which we have observed following laser excitation of the $C\,^3\Pi$–$X\,^3\Delta$ system, and their values have been confirmed by the structure of the $C\,^3\Pi$–$A\,^3\Sigma^-$ transition, which we have found near 8000 Å. The details of these experiments will be reported elsewhere.

A broad-band laser excitation spectrum of the (0,0) sequence of the $B\,^3\Phi$–$X\,^3\Delta$ system of NbN is shown in Fig. 1.

This article is copyrighted as indicated in the article. Reuse of AIP content is subject to the terms at: http://scitation.aip.org/termsconditions. Downloaded to IP: 128.114.34.22 On: Wed, 26 Nov 2014 12:31:44

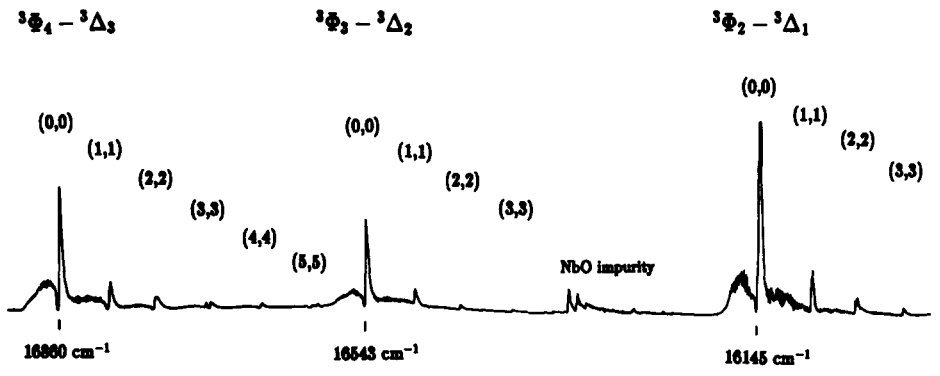

FIG. 1. Broadband laser excitation spectrum of the (0,0) sequence of the $B\,^3\Phi$–$X\,^3\Delta$ transition of NbN.

The spin–orbit structure is seen to be asymmetric, with the $^3\Phi_3$–$^3\Delta_2$ (central) component blue shifted by about 40 cm^{-1} from the midpoint of the pattern. At the same time the $^3\Phi_3$–$^3\Delta_2$ subband is found to be weaker than expected. These two effects result from spin–orbit interaction between the $\sigma\delta$ $a\,^1\Delta_2$ state at 5197 cm^{-1} and the $^3\Delta_2$ component of $\sigma\delta\,X\,^3\Delta$, as we describe below.

IV. ANALYSIS OF THE HYPERFINE STRUCTURE

The Q branch heads of the three spin components of the (0,0) vibrational band are shown in Fig. 2 at sub-Doppler resolution. In all three subbands the hyperfine widths of the rotational lines are largest at low J and decrease as $1/J$, in the manner characteristic of case (a_β) coupling in both electronic states. The patterns can be understood qualitatively from the diagonal elements of the magnetic hyperfine Hamiltonian[5]

$$H_{\rm hfs} = aI_zL_z + b\,\mathbf{I}\cdot\mathbf{S} + cI_zS_z. \tag{2}$$

In a case (a_β) basis these are

$$\langle \Lambda;S\Sigma;J\Omega IF|H_{\rm hfs}|\Lambda;S\Sigma;J\Omega IF\rangle = \frac{[a\Lambda+(b+c)\Sigma]\Omega[F(F+1)-I(I+1)-J(J+1)]}{2J(J+1)}. \tag{3}$$

It is seen in Fig. 2 that the hyperfine widths are much greater in the outer two components ($\Sigma = \pm 1$) than in the central component ($\Sigma = 0$), and that the sense of the hyperfine splitting is opposite in these two outer components. This means that the dominant term in the hyperfine Hamiltonian is $(b+c)$, which is multiplied by Σ in Eq. (3). To be exact the largest hyperfine parameter is found to be the Fermi contact interaction in the $\sigma\delta\,X\,^3\Delta$ state; the Fermi contact

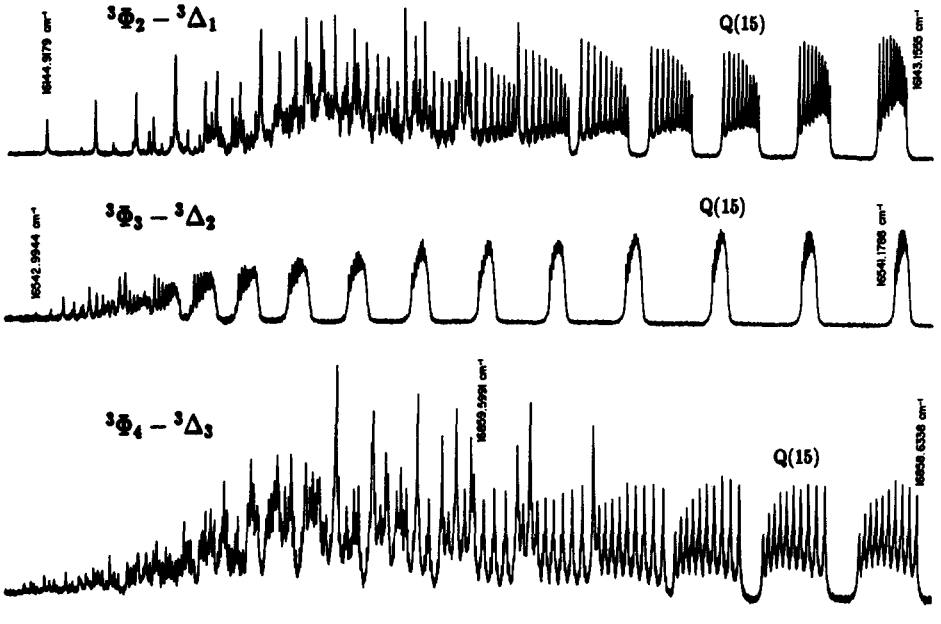

FIG. 2. Sub-Doppler laser-induced fluorescence spectra of the Q heads of the (0,0) band of NbN, $B\,^3\Phi$–$X\,^3\Delta$.

This article is copyrighted as indicated in the article. Reuse of AIP content is subject to the terms at: http://scitation.aip.org/termsconditions. Downloaded to IP: 128.114.34.22 On: Wed, 26 Nov 2014 12:31:44

interaction is part of the parameter b, and its large size shows that the σ unpaired electron is in an orbital derived from the Nb $5s$ atomic orbital. The nonzero splittings in $^3\Phi_3$–$^3\Delta_2$ come from the a **I**·**L** term of Eq. (2). Also consistent with case (a_β) coupling is the fact that the hyperfine widths are largest in the $^3\Phi_4$–$^3\Delta_3$ component, reflecting the coefficient Ω in Eq. (3).

Expanded scale tracings of the $^3\Phi_2$–$^3\Delta_1$ Q head are given in Fig. 3, where it can be seen that the low-J Q lines give extremely complicated patterns. The $Q(2)$ line, for example, covers the full width of Fig. 3(a) (about 0.6 cm^{-1}), and consists of 13 hyperfine lines; these represent all the possible $\Delta F = 0, \pm 1$ transitions between the levels $J = 2$, $F = 2.5$–6.5 in the two electronic states. At low J values the rules of vector coupling limit the number of hyperfine components that can exist, such that the full complement of ten hyperfine levels expected for $I = 9/2$ appears for the first time only at $J = 5$. Each $Q(J)$ line then consists of 28 hyperfine lines according to the selection rule $\Delta F = 0, \pm 1$. Also, at this stage, the hyperfine level splittings in the ground state are becoming small enough that the Doppler profiles of the hyperfine lines overlap, so that crossover resonances (center dips), which are an artifact[12] of the intermodulated fluorescence technique, begin to appear. In principle there can be a center dip between every pair of close hyperfine lines sharing a common lower level, which roughly doubles the number of lines that would appear in the worst case. Fortunately the line strengths of the $\Delta F \neq \Delta J$ hyperfine satellites diminish with increasing J. At $Q(12)$, for instance, the structure has simplified to ten "main" $\Delta F = \Delta J$ hyperfine components, each of which (except the outermost) is flanked on both sides by a center dip between it and its $\Delta F \neq \Delta J$ hyperfine "satellites." The $\Delta F \neq \Delta J$ satellites themselves are not observable because they are far too weak, but the center dips they cause can be seen because the strength of a center dip is proportional to the geometric mean of the strengths of the contributing transitions.[12]

In general we find that the pattern of center dips in the hyperfine structure of a rotational line gives the ΔJ selection rule of the branch that it belongs to. The present transition of NbN is too simple for this information to be needed, but in more complicated systems like the $B\,^4\Pi$–$X\,^4\Sigma^-$ system of NbO[1] it is useful to see how Q branch lines have center dip patterns on both sides of each main hyperfine component, while R and P lines have center dip patterns only on one side; furthermore the center dip patterns in R and P branches are in the opposite sense, though it will probably not be known beforehand which is which. The reason for the appearance of these patterns is that the Q lines consist of $\Delta F - \Delta J = 0$ main hyperfine components plus $\Delta F - \Delta J = \pm 1$ satellites, one on each side, while a P line, for example, consists of a $\Delta F - \Delta J = 0$ main component plus $\Delta F - \Delta J = 1$ and 2 satellites. The line strengths of the $|\Delta F - \Delta J| = 2$ satellites are usually much smaller than those of the $|\Delta F - \Delta J| = 1$ satellites, so that they are often less important, but the point is that in R and P lines all the satellites and center dips occur on the same side of the main line. Examples of R and P lines showing this effect can be seen in Figs. 5 and 8, which will be

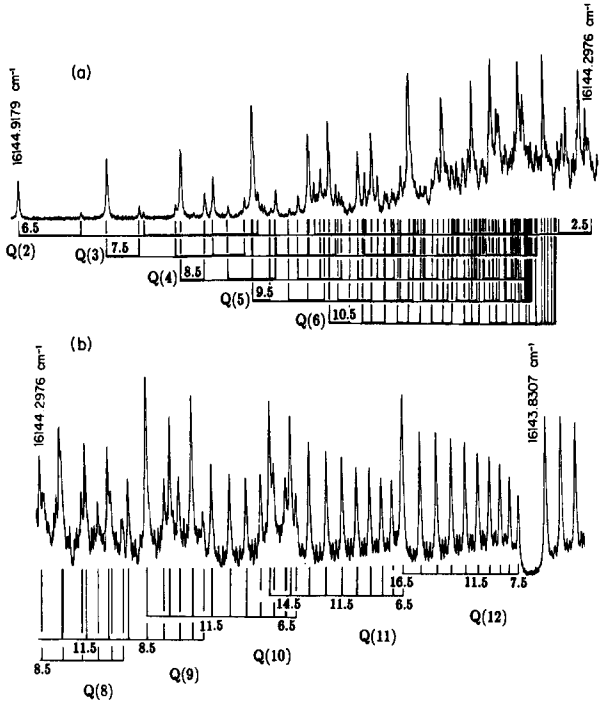

FIG. 3. Assignments of the hyperfine structure in the Q branch head of the $^3\Phi_2$–$^3\Delta_1$ (0,0) subband. (a) The high frequency end. (b) Continuation to lower frequency; the center dip patterns caused by the hyperfine satellites ($\Delta F \neq \Delta J$) produce pairs of weaker lines between the main $\Delta F = \Delta J$ features.

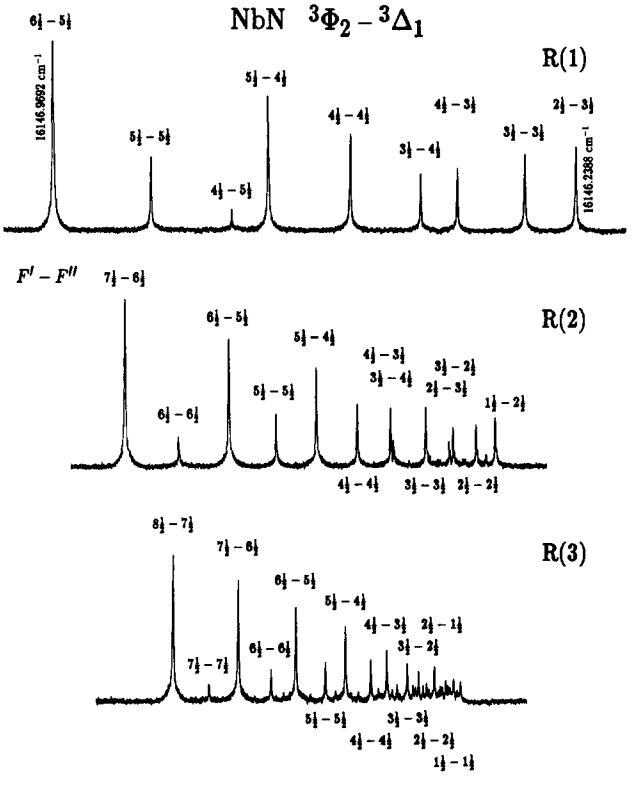

FIG. 4. Hyperfine structures of the lines $R(1)$–$R(3)$ in the $^3\Phi_2$–$^3\Delta_1$, (0,0) subband of NbN. All three tracings are to the same scale.

This article is copyrighted as indicated in the article. Reuse of AIP content is subject to the terms at: http://scitation.aip.org/termsconditions. Downloaded to IP: 128.114.34.22 On: Wed, 26 Nov 2014 12:31:44

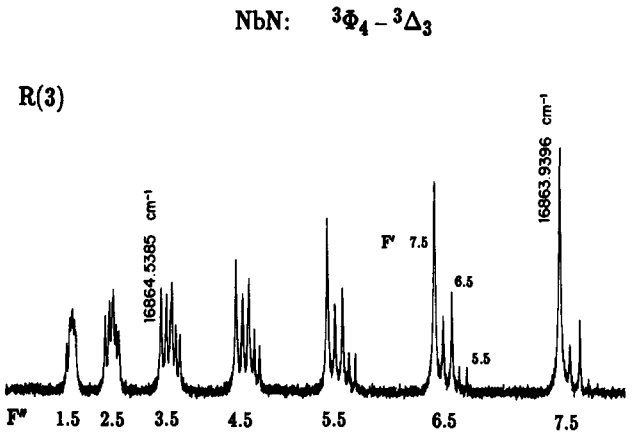

FIG. 5. Hyperfine structure of the $R(3)$ line of the $^3\Phi_4$–$^3\Delta_3$, (0,0) subband. At these low J values the full pattern of ten hyperfine component levels in each state is not developed; the structure consists of seven groups with the same value of F'', each containing three hyperfine components (the central and outer features) and two center dips.

discussed later.

The hyperfine assignments were made by a process of successive refinement of the upper and lower state parameters, beginning with the R branches. Figure 4 shows the first three lines of the R branch of $^3\Phi_2$–$^3\Delta_1$, with their F'–F'' assignments. All nine components permitted by the $\Delta F = 0, \pm 1$ selection rule are clearly seen in $R(1)$. For $R(2)$ 13 of the 15 possible lines have been identified, but already at $R(3)$ the pattern of center dips is becoming sufficiently confused that only 15 of the 21 possible components could be used in the least-squares fit. The first R line of the $^3\Phi_4$–$^3\Delta_3$ subband, $R(3)$, has a very clear pattern of center dips; it is shown in Fig. 5.

The structures of the R lines of $^3\Phi_3$–$^3\Delta_2$ are much narrower, and correspondingly difficult to assign. The lines $R(2)$ to $R(6)$ are shown in Fig. 6. They are complicated by clusters of blended center dips [see, for example, $R(4)$]. The hyperfine energy orders of the components reverse in this J range, so that the $\Delta F = +1$ components, labeled rR in Fig. 6, form a kind of head within the $R(3)$ line, while the $\Delta F = 0$ components (qR) form a sharp line-like feature in $R(5)$. The reason for the confused evolution of the hyperfine structure with J is quite subtle, but worth describing as it is likely to be found quite often. According to Eq. (3) the hyperfine widths decrease as $1/J$ in each state. In this case the hyperfine parameters are fairly similar in the two states, so that the hyperfine widths, as a function of J, can be thought of as two parallel curves with slopes that decrease with J [see Fig. 7(a)]. Now R branch lines correspond to the points J and $J' = J + 1$ on the two curves. It is obvious that at low J, where the curves are falling steeply, the separation of the points J and $J' = J + 1$ may have a sign that is opposite to that at high J, where the curves are nearly flat. It is also clear that the Q branches of this subband cannot show this effect because one curve always lies above the other.

A more dramatic reversal in the sense of the hyperfine structure occurs in all the branches of the two $\Sigma = \pm 1$ (outer) subbands. The Q branch of the $^3\Phi_4$–$^3\Delta_3$ subband is illustrated in Fig. 8. This figure shows how the widths of the Q lines pass through a minimum at $Q(38)$, where the frequency order of the hyperfine components reverses. The corresponding effect occurs in $^3\Phi_2$–$^3\Delta_1$ at $Q(27)$. A reversal of this type means that the hyperfine widths in the two elec-

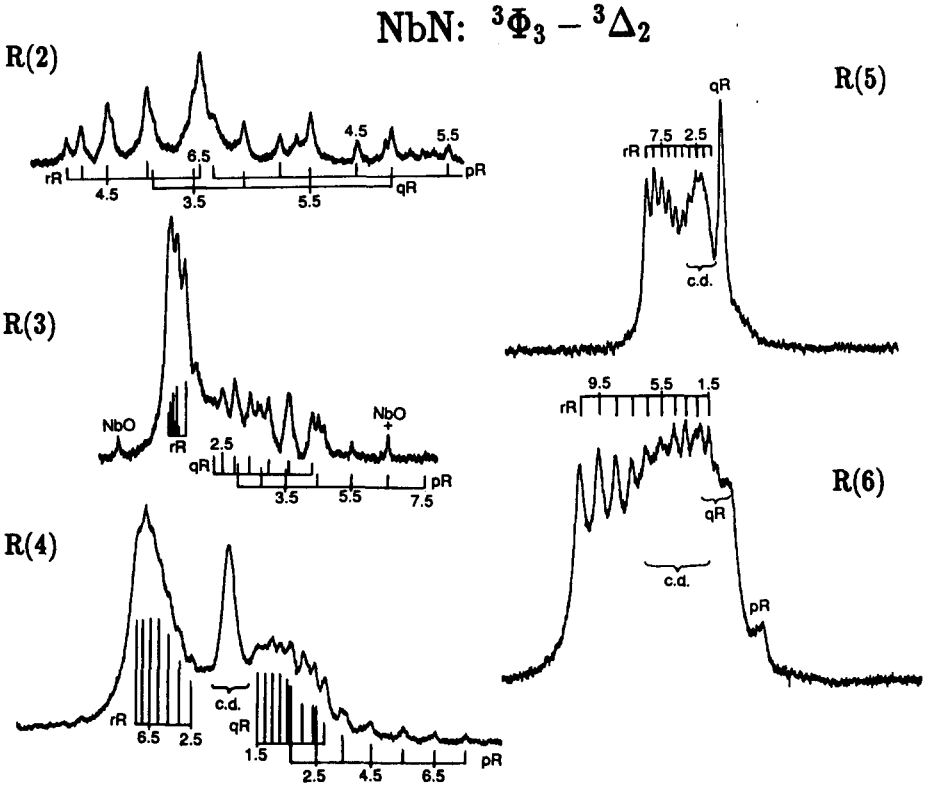

FIG. 6. Evolution of the hyperfine structure in the lines $R(2)$–$R(6)$ of the $^3\Phi_3$–$^3\Delta_2$ (0,0) subband of NbN. The widths of the hyperfine patterns are, respectively, 0.155, 0.098, 0.063, 0.030 and 0.048 cm^{-1}. Symbols such as pR indicate the ΔF and ΔJ selection rules.

This article is copyrighted as indicated in the article. Reuse of AIP content is subject to the terms at: http://scitation.aip.org/termsconditions. Downloaded to IP: 128.114.34.22 On: Wed, 26 Nov 2014 12:31:44

tronic states, which are evolving at different rates with J, happen to be equal at this point. However it can be seen from Eq. (3) that no reversal will occur if both states remain in good case (a) coupling, because the hyperfine widths in the two states will decrease at the same rate, and cannot become equal. In the present case the effect is caused by the ground state. Even though the spin–orbit intervals in the ground state are 400 and 491 cm^{-1}, spin uncoupling, that is the change of spin coupling towards case (b) with increasing rotation, begins to assert itself at J values as low as ~ 10. In the case (b) limit the hyperfine structure of the ground state would be dominated by the Fermi contact interaction, and would be extremely large in the F_1 and F_3 components ($J = N \pm 1$), according to the formula

$$\langle NSJIF|b\,\mathbf{I}\cdot\mathbf{S}|NSJIF\rangle = b\frac{[F(F+1)-I(I+1)-J(J+1)][J(J+1)+S(S+1)-N(N+1)]}{4J(J+1)}. \quad (4)$$

Now since the $X\,^3\Delta$ state is regular the correlation between the level patterns in the case (a) and (b) limits is that $^3\Delta_1$ ($\Sigma = -1$) becomes F_1 ($J = N+1$), while $^3\Delta_3$ ($\Sigma = 1$) becomes F_3 ($J = N-1$). Therefore it can be seen, on comparing Eqs. (3) and (4), that the sense of the hyperfine splitting must change sign in both $^3\Delta_1$ and $^3\Delta_3$. This is illustrated in Fig. 7, where the calculated hyperfine splittings and Q branch linewidths are shown plotted against J.

The rapidity with which the spin-uncoupling sets in is surprising. Figure 7 shows that the hyperfine splitting in $^3\Delta_1$ passes through zero at $J = 14$; this means that spin uncoupling has already contributed enough to cancel the case (a) hyperfine splitting given by Eq. (3). Clearly this is another instance[1,13,14] of the way spin–uncoupling effects become rapidly more important the higher the value of S, because of the factor $[S(S+1) - \Sigma(\Sigma \pm 1)]^{1/2}$ in the matrix element of the "spin-uncoupling operator" $-2B\,\mathbf{J}\cdot\mathbf{S}$ in case (a).

It turns out that the hyperfine energy order must *always* reverse in this fashion in a *regular* triplet state, that is where the spin–orbit parameter A is positive, though *not* in an *inverted* triplet state. Also it will occur for either sign of the Fermi contact parameter b. Whether it is observed or not will depend on the magnitude of A/B, which governs the amount of spin uncoupling and therefore the J value at which the reversal occurs; of course these considerations only apply if the Fermi contact parameter is the largest of the hyperfine parameters.

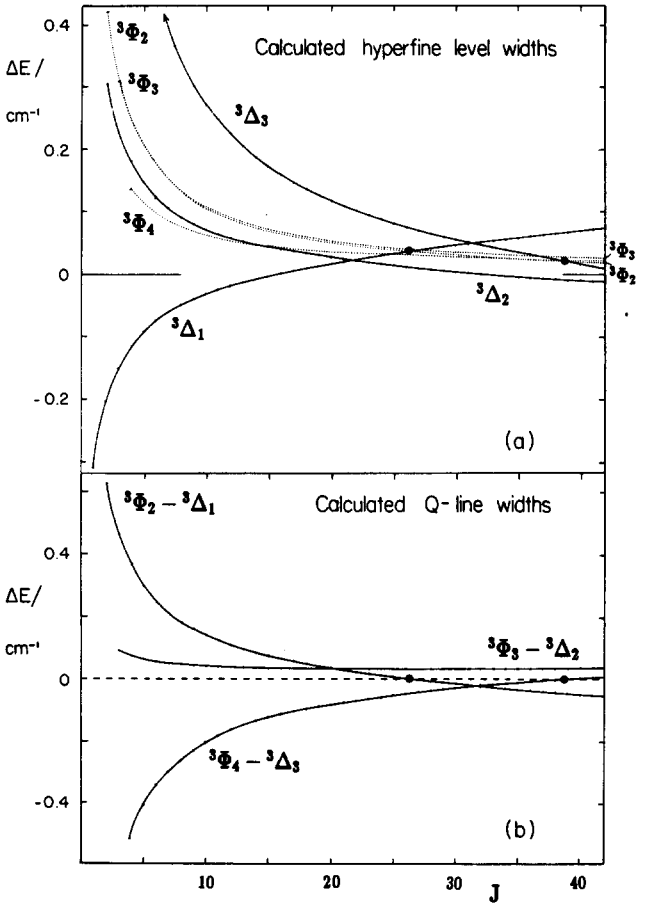

FIG. 7. (a) Calculated hyperfine level widths for the spin components of the $B\,^3\Phi$ and $X\,^3\Delta$ states of NbN. The quantity $E_{hfs}(F=J+I) - E_{hfs}(F=J-I)$ is plotted against J. (b) Calculated Q branch linewidths, obtained by subtracting the $^3\Delta$ level widths of (a) from the $^3\Phi$ level widths. Dots mark points where hyperfine reversals occur.

V. DETERMINATION OF THE MOLECULAR CONSTANTS

The $B\,^3\Phi$ and $X\,^3\Delta$ states of NbN reported in this work are both in "good" case (a) coupling, so that the B–X transition carries no direct information about the spin–orbit intervals. These can, however, be estimated from the differences between the effective B values for the substates, and the values we obtained in this manner are quite similar to those given by Féménias *et al.*[4] We do not give the details because, during the analysis of the B–X system, wavelength-resolved laser-induced fluorescence experiments on the $C\,^3\Pi$–$X\,^3\Delta$ system showed that it contains various weak spin satellite branches as a result of the smaller spin–orbit coupling in the $C\,^3\Pi$ state. Analysis of these satellite branches gave the spin–orbit intervals in the ground state directly, though not with the same precision as the present sub-Doppler measurements of the B–X transition, since they were measured with a grating spectrometer.

Our procedure has therefore been to fix the first- and second-order spin–orbit parameters of the ground state (A and λ) at values that reproduce the separations of the spin satellites of the C–X transition, and to fit the complete sub-Doppler data set of the B–X transition to the differences between the eigenvalues of the rotational and hyperfine Hamiltonians for the $B\,^3\Phi$ and $X\,^3\Delta$ states. The final parameters are not affected by changes in the spin–orbit intervals of the order of the spectrometer accuracy ($\sim 0.2\ cm^{-1}$).

This article is copyrighted as indicated in the article. Reuse of AIP content is subject to the terms at: http://scitation.aip.org/termsconditions. Downloaded to IP: 128.114.34.22 On: Wed, 26 Nov 2014 12:31:44

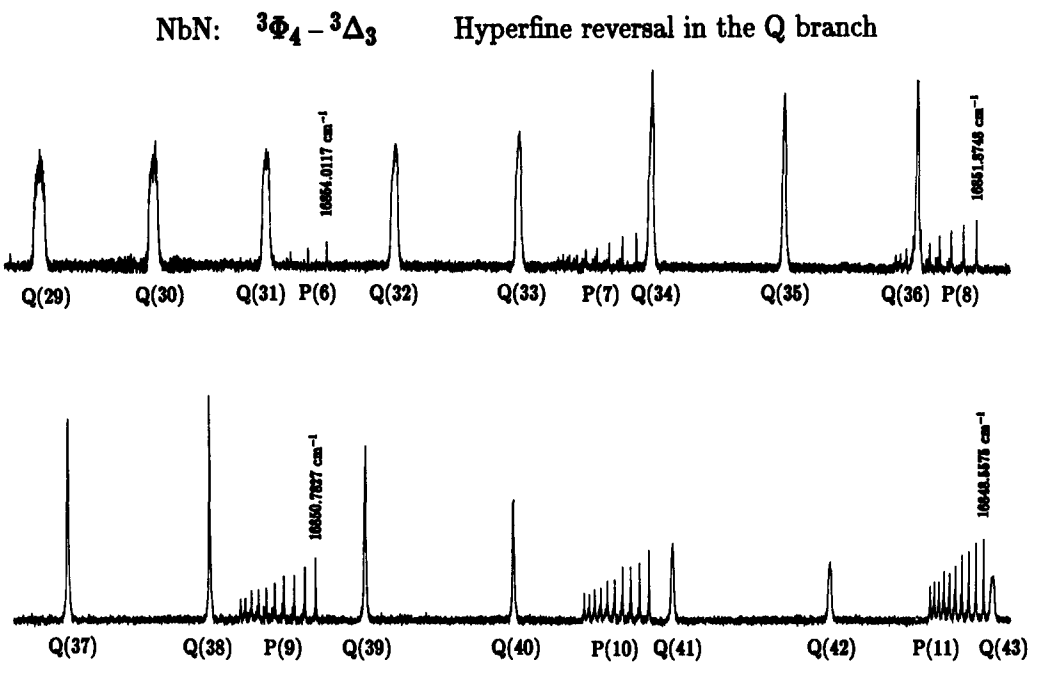

FIG. 8. The NbN spectrum near 16 850 cm^{-1}, showing a reversal in the sense of the hyperfine structure in the Q branch of the $^3\Phi_4$–$^3\Delta_3$ (0,0) subband. The Q branch intensity appears to peak at $Q(38)$, where the hyperfine width is narrowest.

A. Rotational and hyperfine Hamiltonian

The rotational and hyperfine Hamiltonian was based on the standard[15,16] $\mathbf{R}^2$ form which, written using operators appropriate for a case (a_β) basis, is

$$\begin{aligned} H = {} & AL_zS_z + \tfrac{2}{3}\lambda(3S_z^2 - \mathbf{S}^2) + B(\mathbf{J}^2 - J_z^2 + \mathbf{S}^2 - S_z^2) - (B - \tfrac{1}{2}\gamma)(J_+S_- + J_-S_+) \\ & - D(\mathbf{J}^2 - J_z^2 + \mathbf{S}^2 - S_z^2 - J_+S_- - J_-S_+)^2 + \gamma(S_z^2 - \mathbf{S}^2) \\ & + \tfrac{1}{2}A_D[L_zS_z, \mathbf{J}^2 - J_z^2 + \mathbf{S}^2 - S_z^2 - J_+S_- - J_-S_+]_+ \\ & + \tfrac{1}{3}\lambda_D[3S_z^2 - \mathbf{S}^2, \mathbf{J}^2 - J_z^2 + \mathbf{S}^2 - S_z^2 - J_+S_- - J_-S_+]_+ \\ & + aI_zL_z + b\,\mathbf{I}\cdot\mathbf{S} + cI_zS_z + e^2Qq_0(3I_z^2 - \mathbf{I}^2)/[4I(2I-1)]. \end{aligned} \tag{5}$$

The terms in Eq. (5) can be identified by their coefficients. A and λ are the first- and second-order spin–orbit parameters, where λ includes the dipolar electron spin–spin interaction. B is the rotational constant, and D its centrifugal distortion correction; γ is the spin–rotation interaction parameter, and A_D and λ_D represent the centrifugal distortion corrections to the spin–orbit interaction terms. The symbol $[x,y]_+ = xy + yx$ is the anticommutator, which is required to preserve the Hermitian form of the matrices.[17] The last four terms are the magnetic hyperfine terms given in Eq. (2), plus the nuclear electric quadrupole coupling. The matrix elements of the rotational and electron spin parts of H are given in Table I.

Neither the $B\,^3\Phi$ nor the $X\,^3\Delta$ state of NbN actually follows case (a_β) hyperfine coupling, because of extensive spin–orbit contamination, so that we have had to modify Eq. (5). In "pure" case (a_β) coupling the hyperfine matrix elements of Eq. (5) diagonal in Ω are[18]

$$\langle J\Omega IF|H_{\text{mag.hfs}}|J\Omega IF\rangle = \frac{\Omega h\,[F(F+1) - I(I+1) - J(J+1)]}{2J(J+1)}, \tag{6}$$

$$\langle J\Omega IF|H_{\text{mag.hfs}}|J-1,\Omega IF\rangle = -\frac{h\sqrt{J^2-\Omega^2}\sqrt{(J+I+F+1)(F+J-I)(J+I-F)(F+I-J+1)}}{2J\sqrt{(2J+1)(2J-1)}},$$

where h is defined by

$$h = a\Lambda + (b+c)\Sigma. \tag{7}$$

In other words the three Ω substates of a triplet state should have diagonal magnetic hyperfine elements that are given simply[18,19] in terms of the two quantities a and $(b+c)$. We find that Eq. (7) is not obeyed in either state of this transition, and have therefore taken the three h parameters for the three substates as independent parameters. To be sure, Eq. (7) is almost obeyed in the $B\,^3\Phi$ state, but it breaks down completely for the $X\,^3\Delta$ state.

The hyperfine elements off-diagonal in Ω in a "pure" case (a_β) basis,[18]

This article is copyrighted as indicated in the article. Reuse of AIP content is subject to the terms at: http://scitation.aip.org/termsconditions. Downloaded to IP: 128.114.34.22 On: Wed, 26 Nov 2014 12:31:44

$$\langle S\Sigma,J\Omega IF|H_{\text{mag.hfs}}|S\Sigma\pm1,J\Omega\pm1,IF\rangle = b\sqrt{J(J+1)-\Omega(\Omega\pm1)}\sqrt{S(S+1)-\Sigma(\Sigma\pm1)}\times[F(F+1)-I(I+1)-J(J+1)]/[4J(J+1)], \quad (8)$$

$$\langle S\Sigma,J\Omega IF|H_{\text{mag.hfs}}|S\Sigma\pm1,J-1,\Omega\pm1,IF\rangle = \mp b\sqrt{(J\mp\Omega)(J\mp\Omega-1)}\sqrt{S(S+1)-\Sigma(\Sigma\pm1)}\times\frac{\sqrt{(J+I+F+1)(F+J-I)(J+I-F)(F+I-J+1)}}{4J\sqrt{(2J+1)(2J-1)}}$$

contain only the parameter b. In principle, therefore, it is possible to separate b from c (assuming $b+c$ is determinable), if the effects of spin uncoupling are large enough. The two states of NbN described here both have sufficient spin uncoupling that the coefficients in Eq. (8) are determinable. We find that while a single b coefficient suffices for the $B\,^3\Phi$ state, the $X\,^3\Delta$ state requires two different b coefficients, depending on the values of Σ; we define these as b_+ and b_-, for the elements $\langle\Sigma=+1|H|\Sigma=0\rangle$ and $\langle\Sigma=0|H|\Sigma=-1\rangle$, respectively.

To sum up, the $B\,^3\Phi$ state requires four independent magnetic hyperfine parameters, while the $X\,^3\Delta$ state requires five. The $X\,^3\Delta$ state is an example of a major breakdown of the case (a_β) model caused by spin–orbit effects, which is discussed in Sec. VI.

B. Least-squares results

The final set of parameters for the (0,0) band, determined by an iterative least-squares fit, is given in Table II. The data consisted of slightly over 1000 resolved hyperfine transitions (which were all given unit weight) from the three case (a) subbands, and the final standard deviation in the fit was 0.000 58 cm^{-1}. No parts of the data set showed systematic residuals, indicating that the extensions to the hyperfine Hamiltonian form a satisfactory model.

The structures of the Hamiltonian matrices are similar to those outlined in Ref. 19. In the general case, for high J, they are of order 30. Matrix elements of the types $\Delta F=0$, $\Delta J=0,\ \pm1,\ \pm2$ occur; we have not included the matrix elements of the electric quadrupole interaction[18] with $\Delta J\neq0$ for $\Delta\Omega=\pm1$. It has not been necessary to include Λ-doubling effects, so that there is just one matrix for each F value.

The $^3\Phi_2$–$^3\Delta_1$ subbands of the (1,0), (2,1), and (1,1) vibrational bands have been analyzed from Doppler-limited spectra in order to obtain the vibrational frequencies. The hyperfine structure, where it is resolved, is very similar to that of the (0,0) band, and the low J patterns are essentially identical. The model used in the least-squares fit was a simplified case (a) energy expression where the hyperfine effects are omitted: the only parameters varied were effective B and D values for the upper and lower states, and the band origins. The results are given in Table III.

The lists of line frequencies can be found in the theses of two of us (J.A.B. and M.P.J.L.).

VI. SECOND-ORDER SPIN–ORBIT EFFECTS IN THE $X\,^3\Delta$ STATE

A. Asymmetry in the spin–orbit splitting

The comparatively large value of the parameter λ in the $X\,^3\Delta$ ground state (Table II) can be explained almost quantitatively by second-order spin–orbit interaction with the $a\,^1\Delta$ state from the same electron configuration $\sigma\delta$. In the same fashion the distortion of the hyperfine structure which causes the principal departure from the case (a_β) pattern of Eq. (7) can be explained as a cross term between the spin–orbit and Fermi contact interactions.

A comparison of theory and experiment is possible because we have recently observed the $a\,^1\Delta$ state directly, by

TABLE I. Matrix elements of the rotational and electron spin parts of the Hamiltonian for $^3\Phi$ and $^3\Delta$ states, without Λ doubling.[a]

	$\|^3\Delta_3\rangle$	$\|^3\Delta_2\rangle$	$\|^3\Delta_1\rangle$
$\langle^3\Delta_3\|$	$2A+\frac{2}{3}\lambda-\gamma+(B+2A_D+\frac{2}{3}\lambda_D)(x-8)-D(x^2-14x+52)$	$-\sqrt{2(x-6)}\,[B-\frac{1}{2}\gamma+A_D-\frac{1}{3}\lambda_D-2D(x-5)]$	$-2D\sqrt{(x-2)(x-6)}$
$\langle^3\Delta_2\|$		$-2\gamma-\frac{4}{3}\lambda+(B-\frac{4}{3}\lambda_D)(x-2)-D(x^2-12)$	$-\sqrt{2(x-2)}\,[B-\frac{1}{2}\gamma-A_D-\frac{1}{3}\lambda_D-2D(x-1)]$
$\langle^3\Delta_1\|$	Symmetric		$-2A-\gamma+\frac{2}{3}\lambda+(B-2A_D+\frac{2}{3}\lambda_D)x-D(x^2+2x-4)$
	$\|^3\Phi_4\rangle$	$\|^3\Phi_3\rangle$	$\|^3\Phi_2\rangle$
$\langle^3\Phi_4\|$	$3A+\frac{2}{3}\lambda-\gamma+(B+3A_D+\frac{2}{3}\lambda_D)(x-15)-D(x^2-28x+201)$	$-\sqrt{2(x-12)}\,[B-\frac{1}{2}\gamma+\frac{3}{2}A_D-\frac{1}{3}\lambda_D+2D(x-11)]$	$-2D\sqrt{(x-6)(x-12)}$
$\langle^3\Phi_3\|$		$-2\gamma-\frac{4}{3}\lambda+(B-\frac{4}{3}\lambda_D)(x-7)-D(x^2-10x+13)$	$-\sqrt{2(x-6)}\,[B-\frac{1}{2}\gamma-\frac{3}{2}A_D-\frac{1}{3}\lambda_D-2D(x-5)]$
$\langle^3\Phi_2\|$	Symmetric		$-3A+\frac{2}{3}\lambda-\gamma+(B-3A_D+\frac{2}{3}\lambda_D)(x-3)-D(x^2-4x-3)$

[a] The matrices are given in the $\mathbf{R}^2$ formalism, with $x=J(J+1)$.

This article is copyrighted as indicated in the article. Reuse of AIP content is subject to the terms at: http://scitation.aip.org/termsconditions. Downloaded to IP: 128.114.34.22 On: Wed, 26 Nov 2014 12:31:44

TABLE II. Rotational and hyperfine constants for the $B\,^3\Phi$–$X\,^3\Delta$ (0,0) band of NbN.[a] Values in cm^{-1}.

	$B\,^3\Phi$		$X\,^3\Delta$	
T_0	16 518.556 5	± 11	0	fixed
A	269.129 0	2	224.28	fixed
λ	2.715 5	7	22.98	fixed
B	0.495 813 4	15	0.501 464 1	± 15
10^7D	4.867 5	13	4.541 4	7
γ	0.023 07	79	− 0.045 23	10
10^4A_D	− 0.386	9	− 0.430	10
$10^4\lambda_D$	0.487	14	0.381	14
$h(\Sigma = 1)$	0.016 85	8	0.111 27	10
$h(\Sigma = 0)$	0.041 07	13	0.045 86	18
$h(\Sigma = -1)$	0.063 28	8	− 0.061 57	12
b	− 0.021 8	19	...	
b_+	...		0.069 5	10
b_-	...		0.088 1	8
e^2Qq_0	0.000 2	9	0.004 1	8
Derived hyperfine parameters in cm^{-1} (see the text)				
$a\Lambda$[b]	0.040 07		0.024 85	
$b + c$[c]	− 0.023 22		0.086 42	

[a] Errors quoted are one standard deviation, in units of the last significant figure given. $\sigma = 0.000\,58\ cm^{-1}$.
[b] $\frac{1}{2}[h(\Sigma = 1) + h(\Sigma = -1)]$; in pure case ($a_\beta$) coupling this should equal $h(\Sigma = 0)$.
[c] $\frac{1}{2}[h(\Sigma = 1) - h(\Sigma = -1)]$; $c(B\,^3\Phi) = -0.0014\ cm^{-1}$.

wavelength-resolved fluorescence, following laser excitation to the $C\,^3\Pi_1$ state. The energy pattern of $a\,^1\Delta$ and $X\,^3\Delta$ is given in Fig. 9. We begin by taking the electronic wave functions in the single configuration approximation as

$$
\begin{aligned}
|^3\Delta_2\rangle &= |\sigma\delta;2^{-1/2}(\alpha\beta + \beta\alpha)\rangle;\\
|^1\Delta_2\rangle &= |\sigma\delta;2^{-1/2}(\alpha\beta - \beta\alpha)\rangle,\\
|^3\Delta_1\rangle &= |\sigma\delta;\beta\beta\rangle;\\
|^3\Delta_3\rangle &= |\sigma\delta;\alpha\alpha\rangle. \qquad (9)
\end{aligned}
$$

The nonzero matrix elements of the spin-orbit operator between these functions are

$$
\begin{aligned}
\left\langle {}^3\Delta_2 \left| \sum_i a_i \mathbf{l}_i \cdot \mathbf{s}_i \right| {}^1\Delta_2 \right\rangle &= -a_\delta,\\
\left\langle {}^3\Delta_3 \left| \sum_i a_i \mathbf{l}_i \cdot \mathbf{s}_i \right| {}^3\Delta_3 \right\rangle &= -\left\langle {}^3\Delta_1 \left| \sum_i a_i \mathbf{l}_i \cdot \mathbf{s}_i \right| {}^3\Delta_1 \right\rangle = a_\delta. \qquad (10)
\end{aligned}
$$

The two parts of Eq. (10) show that a_δ can be calculated either from the shift caused in the position of $^3\Delta_2$, or from the spin–orbit splitting between $^3\Delta_1$ and $^3\Delta_3$. Experimentally the two values are found to agree within a few percent.

The logic is as follows. The experimental separation of 891.3 cm^{-1} between $^3\Delta_3$ and $^3\Delta_1$, which is $2a_\delta$, gives the value $a_\delta = 446\ cm^{-1}$. If we then assume that $^3\Delta_2$ has been pushed down from the exact midpoint of the $^3\Delta$ manifold by the $^3\Delta_2/^1\Delta$ interaction we see from Fig. 9 that its shift is 46 cm^{-1}. (This is equal to twice the value of λ from Table II.) Presumably the $^1\Delta$ state has been pushed up by this amount also, so we can calculate the diagonal elements of the 2×2 matrix for the interaction of $^3\Delta_2$ with $^1\Delta$, and obtain the unperturbed positions of $^3\Delta$ and $^1\Delta$, as shown on the left-hand side of Fig. 9. Knowing the diagonal elements (H_{11} and H_{22}) and the eigenvalues (λ_1 and λ_2), we can "undiagonalize" the matrix by the formula

$$
|H_{12}| = \tfrac{1}{2}\sqrt{(\lambda_1 - \lambda_2)^2 - (H_{11} - H_{22})^2} \qquad (11)
$$

to obtain the off-diagonal element, which is $a_\delta = H_{12} = 467$ cm^{-1}. The agreement between the values of a_δ is remarkable, considering the simplicity of the model but, as we show below, we do not expect it to be perfect because the hyperfine structure indicates that there are further spin–orbit effects contaminating the ground state.

TABLE III. Rotational constants from the $^3\Phi_2$–$^3\Delta_1$ subbands of other vibrational bands of the $B\,^3\Phi$–$X\,^3\Delta$ system of NbN.[a] Values in cm^{-1}.

	v'	v''	T_0	B'	$10^7D'$	B''	$10^7D''$
$^3\Phi_2$–$^3\Delta_1$	1	0	17 130.999(3)	0.492 30(6)	4.94(31)	0.500 14(6)	4.49(32)
	2	1	17 075.115(2)	0.489 94(6)	5.55(37)	0.497 67(6)	5.24(37)
	1	1	16 097.260(4)	0.492 51(8)	4.52(40)	0.497 48(8)	4.11(42)

[a] Error limits are one standard deviation, in units of the last significant figure quoted. The energy expression used contained no terms in Ω, so that T_0 is the hypothetical $Q(0)$ line position. The rms errors (σ) were 0.003, 0.002, and 0.004 cm^{-1}, respectively.

This article is copyrighted as indicated in the article. Reuse of AIP content is subject to the terms at: http://scitation.aip.org/termsconditions. Downloaded to IP: 128.114.34.22 On: Wed, 26 Nov 2014 12:31:44

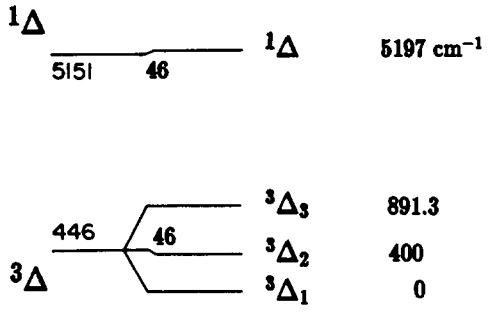

FIG. 9. Energy level patterns of the $X\,^3\Delta$ and $a\,^1\Delta$ $v=0$ levels of NbN, indicating the effects of spin–orbit interaction.

B. The hyperfine *h* parameters

Just as the spin–orbit operator, in the microscopic form of Eq. (10), has matrix elements between the $^3\Delta$ and $^1\Delta$ states, so do the Fermi contact and dipolar hyperfine interactions. The relevant parts of the Hamiltonian can be written

$$H = H_{\text{spin-orbit}} + H_{\text{mag.hfs}}$$

$$= \sum_i a_i \mathbf{l}_i \cdot \mathbf{s}_i + \sum_i b_i \mathbf{I} \cdot \mathbf{s}_i + \sum_i c_i I_z s_{iz}, \tag{12}$$

where a_i is a spin–orbit parameter,[20] not to be confused with the coefficient of $\mathbf{I}\cdot\mathbf{L}$ in the magnetic hyperfine Hamiltonian,[5] and b_i and c_i represent the Fermi contact and dipolar interactions; the subscript i indicates the unpaired electrons. The matrix elements of Eq. (12) in the electronic basis of Eq. (9), which omits the functions on which the nuclear spin operators act, are

$$\begin{aligned}\langle {}^3\Delta_2 | H | {}^1\Delta_2 \rangle &= -a_\delta + \tfrac{1}{2}(b_\sigma - c_\delta) I_z, \\ \langle {}^3\Delta_3 | H | {}^3\Delta_3 \rangle &= -\langle {}^3\Delta_1 | H | {}^3\Delta_1 \rangle \\ &= a_\delta + \tfrac{1}{2}(b_\sigma + c_\delta) I_z. \end{aligned} \tag{13}$$

It is assumed here that the Fermi contact parameter comes entirely from the σ electron and, likewise, that the dipolar parameter comes only from the δ electron.

We can identify the coefficient $\frac{1}{2}(b_\sigma + c_\delta)$ with the term $(b+c)$ appearing in the h parameters of Eq. (7), since the factor of 1/2 comes from the fact that there are two unpaired electrons present. Clearly the coefficient $\frac{1}{2}(b_\sigma - c_\delta)$ in the off-diagonal element in Eq. (13) is equal to $(b-c)$, but unfortunately it is not easy to obtain $(b-c)$ experimentally. In principle, as we have explained, b can be separated from c using the hyperfine contribution to the spin-uncoupling matrix elements, given in Eq. (8); in practice, Table II shows that b is not well defined in the $X\,^3\Delta$ state. It also appears that c is nonzero because the difference between $h(^3\Delta_1)$ and $h(^3\Delta_3)$ does not correspond to the average of b_+ and b_-; for instance

$$\tfrac{1}{2}[h(^3\Delta_3) - h(^3\Delta_1)] = 0.086\,42\ \text{cm}^{-1} = \text{“}b + c\text{”}, \tag{14}$$

while

$$\tfrac{1}{2}(b_+ + b_-) = 0.0788\ \text{cm}^{-1} = \text{“}b\text{”}. \tag{15}$$

However, the fact that b_+ and b_- are not equal suggests that there are probably further spin–orbit effects contaminating the $X\,^3\Delta$ state, so that there is probably little point in attempting to determine c or $(b-c)$ from Eqs. (14) and (15).

On the other hand, Eq. (7) shows that the h parameter of the $^3\Delta_2$ component should be the average of $h(^3\Delta_3)$ and $h(^3\Delta_1)$, assuming these to be unperturbed. This gives

$$\tfrac{1}{2}[h(^3\Delta_3) + h(^3\Delta_1)] = 0.024\,85\ \text{cm}^{-1} = a\Lambda \tag{16}$$

which is to be compared to the experimental value 0.045 86 cm^{-1}. Evidently the difference must come from the cross term between the spin–orbit and hyperfine parts of the off-diagonal element in Eq. (13). This could be handled by second-order perturbation theory, where the calculated correction is

$$h(^3\Delta_2) - a\Lambda = -2a_\delta(b-c)/[E^0(^3\Delta) - E^0(^1\Delta)]. \tag{17}$$

Alternatively it can be treated more exactly by transforming the matrix of $(b-c)$ in the electronic basis

$$\begin{bmatrix} |^1\Delta\rangle \\ |^3\Delta_2\rangle \end{bmatrix}$$

to the basis in which the spin–orbit interaction is diagonal, since we have the appropriate eigenvectors from the “undiagonalization” of Eq. (11). We have therefore made the approximation that the hyperfine parameter c is negligible, and find

$$\begin{bmatrix} c & s \\ -s & c \end{bmatrix} \begin{bmatrix} 0 & 0.086\,42 \\ 0.086\,42 & 0 \end{bmatrix} \begin{bmatrix} c & -s \\ s & c \end{bmatrix} = \begin{bmatrix} -0.016\,83 & 0.084\,77 \\ 0.084\,77 & 0.016\,83 \end{bmatrix}. \tag{18}$$

Equation (18) shows that the cross term between the spin–orbit and Fermi contact interactions should raise the apparent value of $h(^3\Delta_2)$ by 0.016 83 cm^{-1}. Experimentally the correction is

$$h(^3\Delta_2) - \tfrac{1}{2}[h(^3\Delta_3) + h(^3\Delta_1)] = 0.021\,01\ \text{cm}^{-1} \tag{19}$$

which is in very satisfactory agreement, considering the simplicity of the model used.

In terms of an effective Hamiltonian the consequence of the second-order spin–orbit/Fermi contact cross term is to modify[21] the value of a, the coefficient of $\mathbf{I}\cdot\mathbf{L}$ in the magnetic hyperfine Hamiltonian given as Eq. (2). Even without doing any algebra it is obvious that this would be the consequence, because the combination of operators $(\mathbf{L}\cdot\mathbf{s}_i)(\mathbf{I}\cdot\mathbf{s}_j)$ can be recoupled[22] by standard tensor methods to give (among other things) a multiple of $(\mathbf{s}_i\cdot\mathbf{s}_j)(\mathbf{I}\cdot\mathbf{L})$: the recoupled operator will give a Σ-dependent correction to the coefficient of the diagonal term $I_z L_z$.

There should be an equal and opposite correction to the h value of the $^1\Delta$ state. If it is assumed that $h(^1\Delta) = a\Lambda$, taking the value from Eq. (16) since it comes from the same electron configuration as $X\,^3\Delta$, we see that the correction would reduce the experimental value almost to zero. It will be interesting to verify this point by observation, but so far we have not been able to obtain sub-Doppler spectra involving this state. It is also worth noting that *ab initio* calculations of the hyperfine parameters could be considerably in error if these second-order effects are not treated appropriately.

Second-order perturbation theory indicates that there

This article is copyrighted as indicated in the article. Reuse of AIP content is subject to the terms at: http://scitation.aip.org/termsconditions. Downloaded to IP: 128.114.34.22 On: Wed, 26 Nov 2014 12:31:44

will be a correction to the quadrupole coupling parameter of the ground state, arising from the off-diagonal elements of the Fermi contact interaction. However order-of-magnitude considerations based on Eq. (13) show that the expected correction is much too small to be observable.

VII. DISCUSSION

This work represents one of the most detailed accounts yet reported of the hyperfine structure in an electronic transition between states in apparently good case (a) coupling; it has provided excellent examples of the appearance and behavior of hyperfine structure in a high multiplicity situation. Particular attention has been paid to the calibration, so that the standard deviation in the least-squares fit is exceptionally low, and the results are of higher than usual precision.

The most interesting aspects are the second-order spin–orbit effects. Because we now have the absolute energies of the various spin–orbit states involved (which were not available in Ref. 4) we can treat these effects quantitatively. It can be shown that the asymmetry in the ground state spin–orbit pattern is explained, almost exactly, in terms of interaction between $^3\Delta_2$ and $^1\Delta$, and furthermore that the hyperfine structure in such a situation is distorted by cross terms between the spin–orbit and Fermi contact interactions. The $X\,^3\Delta$ state is a very clear instance of a major breakdown of the case (a_β) model for the hyperfine structure, which occurs as a result of spin–orbit interaction in a $4d$ metal system.

This work has cleared up essentially all the problems remaining unanswered in the rotational analysis presented in Ref. 4 from lower resolution spectra, and confirms that both electronic states are regular, rather than inverted as suggested in Ref. 11. The main point that emerges on comparing the present results with Ref. 4 is that the estimation of the spin–orbit intervals from the difference between the rotational constants for the various Ω substates may not always be as precise as might be thought. For instance Mulliken's formula[23]

$$B_{\mathrm{eff},\Sigma} = B(1 + 2B\Sigma/A\Lambda) \qquad (20)$$

leads to an estimate of the spin–orbit parameter A for the $X\,^3\Delta$ state[4] which is only 80% of the actual value. There is no question of the validity of Eq. (20) in the case (a) limit; what is happening here is that, in a situation where the differences between the $B_{\mathrm{eff},\Sigma}$ values are quite small, fairly minor spin–orbit contaminations by distant states will have a major effect on the applicability of Eq. (20). In our case, where the spin–orbit parameters are known, these minor contaminations are absorbed by the effective Hamiltonian into the centrifugal distortion corrections to the spin parameters, A_D and λ_D. There is no doubt that these contaminations are present, because A_D and λ_D are of the order of several percent of the differences between the $B_{\mathrm{eff},\Sigma}$ values; also the fact that the off-diagonal magnetic hyperfine parameters $b_+ = \langle\Sigma = 1|H|\Sigma = 0\rangle$ and $b_- = \langle\Sigma = 0|H|\Sigma = -1\rangle$ are different in the $X\,^3\Delta$ state indicates that the case (a) electronic basis states $|\eta\Lambda; S\Sigma\rangle$ are not "pure," even allowing for the large $^3\Delta_2/^1\Delta$ interaction.

The incorrect signs for the spin–orbit coupling derived by Pazyuk *et al.* turn out to arise from their assignment of subbands of the nearby $C\,^3\Pi$–$X\,^3\Delta$ transition as case (a)-forbidden spin satellites of the $B\,^3\Phi$–$X\,^3\Delta$ system. The spin–orbit structure of the $C\,^3\Pi$ state is in fact highly distorted by interaction with the $^1\Pi$ state from the same configuration, $\pi\delta$. We have recently completed an analysis of the hyperfine structure in the $C\,^3\Pi$ state and, as expected, it is even more irregular than that in the $X\,^3\Delta$ state: the details will be published elsewhere.

The vibrational frequency of the $X\,^3\Delta_1$ substate of NbN is $\Delta G_{1/2} = 1033.739\ \mathrm{cm}^{-1}$ (as derived from Tables II and III). This is 3.1% higher than the value $1002.5\ \mathrm{cm}^{-1}$ observed in an argon matrix.[24] As explained by Jacox,[25] the higher the percentage gas-minus-matrix shift for the vibrational frequency, the more ionic the molecule is, in general. By comparison,[25] the corresponding shifts for NbO and CeO are 1.4% and 2.0%, so that NbN is fairly highly ionic: it will be instructive to measure its electric dipole moment.

ACKNOWLEDGMENTS

We thank the Natural Sciences and Engineering Research Council of Canada for financial support, and acknowledgement is made to the donors of the Petroleum Research Fund, administered by the American Chemical Society, for partial support of this research. J.O.S. thanks the Deutsche Forschungsgemeinschaft for a postdoctoral fellowship which enabled him to spend part of 1986 at the University of British Columbia. J.L.F. thanks the Conseil Général des Alpes-Maritimes (France) for partial support of this work.

[1] J.-L. Féménias, G. Cheval, A. J. Merer, and U. Sassenberg, J. Mol. Spectrosc. **124**, 348 (1987).
[2] T. M. Dunn, in *Molecular Spectroscopy: Modern Research*, edited by K. Narahari Rao and C. W. Mathews (Academic, New York, 1972), p. 231.
[3] G. Cheval, J.-L. Féménias, A. J. Merer, and U. Sassenberg, J. Mol. Spectrosc. **131**, 113 (1988).
[4] J.-L. Féménias, Ch. Athénour, K. M. Rao, and T. M. Dunn, J. Mol. Spectrosc. **130**, 269 (1988).
[5] R. A. Frosch and H. M. Foley, Phys. Rev. **86**, 1337 (1952).
[6] M. S. Sorem and A. L. Schawlow, Opt. Commun. **5**, 148 (1972).
[7] S. Gerstenkorn and P. Luc, *Atlas du Spectre d'Absorption de la Molécule d'Iode* (CNRS, Paris, France, 1978); S. Gerstenkorn and P. Luc, Rev. Phys. Appl. **14**, 791 (1979).
[8] A. S-C. Cheung, R. C. Hansen, and A. J. Merer, J. Mol. Spectrosc. **91**, 165 (1982).
[9] T. M. Dunn and K. M. Rao, Nature (London) **222**, 268 (1969).
[10] J.-L. Féménias, C. Athénour, and T. M. Dunn, J. Chem. Phys. **63**, 2861 (1975).
[11] E. A. Pazyuk, E. N. Moskvitina, and Yu. Ya. Kuzyakov, Spectrosc. Lett. **19**, 627 (1986).
[12] M. S. Sorem, T. W. Hänsch, and A. L. Schawlow, Chem. Phys. Lett. **17**, 300 (1972).
[13] U. Sassenberg, A. S-C. Cheung, and A. J. Merer, Can. J. Phys. **62**, 1610 (1984).
[14] A. J. Merer, G. Huang, A. S-C. Cheung, and A. W. Taylor, J. Mol. Spectrosc. **125**, 465 (1987).
[15] J. H. Van Vleck, Rev. Mod. Phys. **23**, 213 (1951).
[16] R. N. Zare, A. L. Schmeltekopf, W. J. Harrop, and D. L. Albritton, J. Mol. Spectrosc. **46**, 37 (1973).
[17] J. M. Brown, E. A. Colbourn, J. K. G. Watson, and F. D. Wayne, J. Mol. Spectrosc. **74**, 294 (1979).
[18] A. Carrington, P. N. Dyer, and D. H. Levy, J. Chem. Phys. **47**, 1756 (1967).

This article is copyrighted as indicated in the article. Reuse of AIP content is subject to the terms at: http://scitation.aip.org/termsconditions. Downloaded to IP: 128.114.34.22 On: Wed, 26 Nov 2014 12:31:44

[19]J. M. Brown, I. Kopp, C. Malmberg, and B. Rydh, Phys. Scr. **17**, 55 (1978).
[20]I. Kovács, Can. J. Phys. **36**, 309 (1958).
[21]A. S-C. Cheung and A. J. Merer, Mol. Phys. **46**, 111 (1982).
[22]B. L. Silver, *Irreducible Tensor Methods* (Academic, New York, 1976).
[23]G. Herzberg, *Spectra of Diatomic Molecules*, 2nd ed. (Van Nostrand, Princeton, 1950), p. 235.
[24]D. W. Green, W. Korfmacher, and D. M. Gruen, J. Chem. Phys. **58**, 404 (1973).
[25]M. E. Jacox, J. Mol. Spectrosc. **113**, 286 (1985).

This article is copyrighted as indicated in the article. Reuse of AIP content is subject to the terms at: http://scitation.aip.org/termsconditions. Downloaded to IP: 128.114.34.22 On: Wed, 26 Nov 2014 12:31:44